Unsymmetrical 1,4-Diazabutadiene Complexes of Platinum(II)

Kaiyuan Yang, Rene J. Lachicotte, and Richard Eisenberg*

Department of Chemistry, University of Rochester, Rochester, New York 14627

Received May 30, 1997[⊗]

The new unsymmetrical 1,4-diazabutadiene ligand glyoxal bis(2-(methoxymethyl)-4,6-di-*tert*-butylphenyl)diimine (**L**) and its reduced analog (**LH_4**) were synthesized. The reactions of both ligands with bis(benzonitrile) complexes of palladium and platinum, $MCl_2(PhCN)_2$, were investigated. Two isomers of formula MCl_2**L** were isolated from the reaction of **L** with $MCl_2(PhCN)_2$ (**1a** and **1b** for Pd, **2a** and **2b** for Pt), while only a single product, MCl_2(**LH_4**), formed in the reaction with **LH_4** (**3** for M = Pd, **4** for M = Pt). All new compounds were characterized by elemental analyses and IR and NMR spectroscopies. The molecular structures for **L**, **LH_4**, **2b**, **3**, and **4** were determined by single-crystal X-ray diffraction. The metal complexes exhibit distorted square-planar geometry. The aryl groups of the **L** and **LH_4** ligands lie out of the coordination plane in a manner that blocks potential axial ligation sites. Ligand **L** crystallizes in the triclinic space group $P\bar{1}$ with $a = 5.760(1)$ Å, $b = 9.383(2)$ Å, $c = 14.954(3)$ Å, $\alpha = 89.38(2)°$, $\beta = 79.67(2)°$, $\gamma = 88.14(2)°$, and Z = 1. The reduced ligand **LH_4** crystallizes in the monoclinic space group $P2_1$ with $a = 5.9758(1)$ Å, $b = 17.4272(2)$ Å, $c = 15.6222(1)$ Å, $\beta = 99.063(1)°$, and Z = 2. Complex **2b** crystallizes in the monoclinic space group $P2_1/c$ with $a = 16.9599(2)$ Å, $b = 18.4985(2)$ Å, $c = 12.4976(0)$ Å, $\beta = 100.945(0)°$, and Z = 4. Complex **3** crystallizes in the monoclinic space group $C2/c$ with $a = 36.1506(8)$ Å, $b = 8.0994$ (2) Å, $c = 15.5671(1)$ Å, $\beta = 113.988(1)°$, and Z = 4. Complex **4** crystallizes in the monoclinic space group $C2/c$ with $a = 36.0649(3)$ Å, $b = 8.1787(2)$ Å, $c = 15.7585(3)$ Å, $\beta = 112.610(1)°$, and Z = 4.

Introduction

The recent discovery by Brookhart and co-workers of Ni(II) and Pd(II) α-olefin polymerization catalysts containing bulky diimine ligands[1−9] has stimulated renewed interest in the chemistry of 1,4-diazabutadiene (DAB) ligands and their complexes.[10−15] Ligands of this

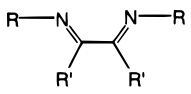

DAB

type have been studied extensively in several different contexts. First, DAB ligands possess different possible modes of coordination as 2-, 4-, 6-, and even 8-electron donors in terminal, chelating, and bridging arrangements.[16−20] These different modes of coordination in turn confer different reactivities on the complexed metal ions, as detailed in the review by van Koten and Vrieze.[10] Second, as α-diimine ligands, DAB ligands have electronic structural similarities to the more extensively studied heteroaromatic chelating agents 2,2′-bipyridine and 1,10-phenanthroline.[21,22] In 1973, for example, Miller and Dance[23] showed that square-planar Ni(II) diimine dithiolate complexes containing 1,10-phenanthroline and the DAB ligand biactetyl bis(anil) (R = Ph; R′ = Me) were spectroscopically similar with a common low-energy charge transfer-to-diimine absorption.

In this paper, we report the syntheses of an unsymmetrical DAB ligand, its saturated analog, and their Pt(II) and Pd(II) dichloro complexes. The ligand synthesis was originally undertaken to generate a tetradentate chelating agent that would bind to a six-coordinate

[⊗] Abstract published in *Advance ACS Abstracts,* November 1, 1997.

(1) Brookhart, M.; Lincoln, D. M. *J. Am. Chem. Soc.* **1988**, *110*, 8719.
(2) Brookhart, M.; Volpe, A. F.; Lincoln, D. M.; Hovarth, I. T.; Millar, J. M. *J. Am. Chem. Soc.* **1990**, *112*, 5634.
(3) Brookhart, M.; Rix, F. C.; DeSimone, J. M.; Barborak, J. C. *J. Am. Chem. Soc.* **1992**, *114*, 5894−5895.
(4) Brookhart, M.; Hauptman, E. *J. Am. Chem. Soc.* **1992**, *114*, 4437.
(5) Brookhart, M.; Rix, F. C.; DeSimone, J. M.; Barborak, J. C. *J. Am. Chem. Soc.* **1992**, *114*, 5894.
(6) Brookhart, M.; Hauptman, E.; Lincoln, D. *J. Am. Chem. Soc.* **1992**, *114*, 10394.
(7) Rix, F. C.; Brookhart, M. *J. Am. Chem. Soc.* **1995**, *117*, 1137.
(8) Rix, F. C.; Brookhart, M.; White, P. S. *J. Am. Chem. Soc.* **1996**, *118*, 4746−4764.
(9) Rix, F. C.; Brookhart, M.; White, P. S. *J. Am. Chem. Soc.* **1996**, *118*, 2436−2448.
(10) van Koten, G.; Vrieze, K. *Adv. Organomet. Chem.* **1982**, *21*, 151−239.
(11) Klein, R. A.; Hartl, F.; Elsevier, C. J. *Organometallics* **1997**, *16*, 1284−1291.
(12) van Asselt, R.; Elsevier, C. J.; Amatore, C.; Jutand, A. *Organometallics* **1997**, *16*, 317−328.
(13) van Asselt, R.; Vrieze, K.; Elsevier, C. J. *J. Organomet. Chem.* **1994**, *480*, 27−40.
(14) Groen, J. H.; Delis, J. G. P.; van Leeuwen, W. N. M.; Vrieze, K. *Organometallics* **1997**, *16*, 68−77.
(15) Groen, J. H.; Elsevier, C. J.; Vrieze, K.; Smeets, W. J. J.; Spek, A. L. *Organometallics* **1996**, *15*, 3445−3455.
(16) van der Poel, H.; van Koten, G.; Vrieze, K. *Inorg. Chem.* **1980**, *19*, 1145.
(17) Frühauf, H. W.; Landers, R.; Goddard, R.; Krüger, C. *Angew. Chem.* **1978**, *90*, 56.
(18) Staal, L. H.; van Koten, G.; Vrieze, K.; Ploeger, F.; Stam, C. H. *Inorg. Chem.* **1982**, *20*, 1830.
(19) van der Poel, H.; van Koten, G.; Vrieze, K.; Kokkes, M.; Stam, C. H. *J. Organomet. Chem.* **1979**, *175*, C21.
(20) Shi, Q. Z.; Richmond, T. G.; Trogler, W. C.; Basolo, F. *Organometallics* **1982**, *1*, 1033−1037.
(21) McWhinnie, W. R.; Miller, J. D. *Adv. Inorg. Chem. Radiochem.* **1969**, *12*, 135−215.
(22) Cotton, F. A.; Wilkinson, G. *Advanced Inorganic Chemistry*, 5th ed.; John Wiley and Sons, Inc.: New York, 1988; p 1455.
(23) Miller, T. R.; Dance, G. *J. Am. Chem. Soc.* **1973**, *95*, 6970.

S0276-7333(97)00452-4 CCC: $14.00

Scheme 1

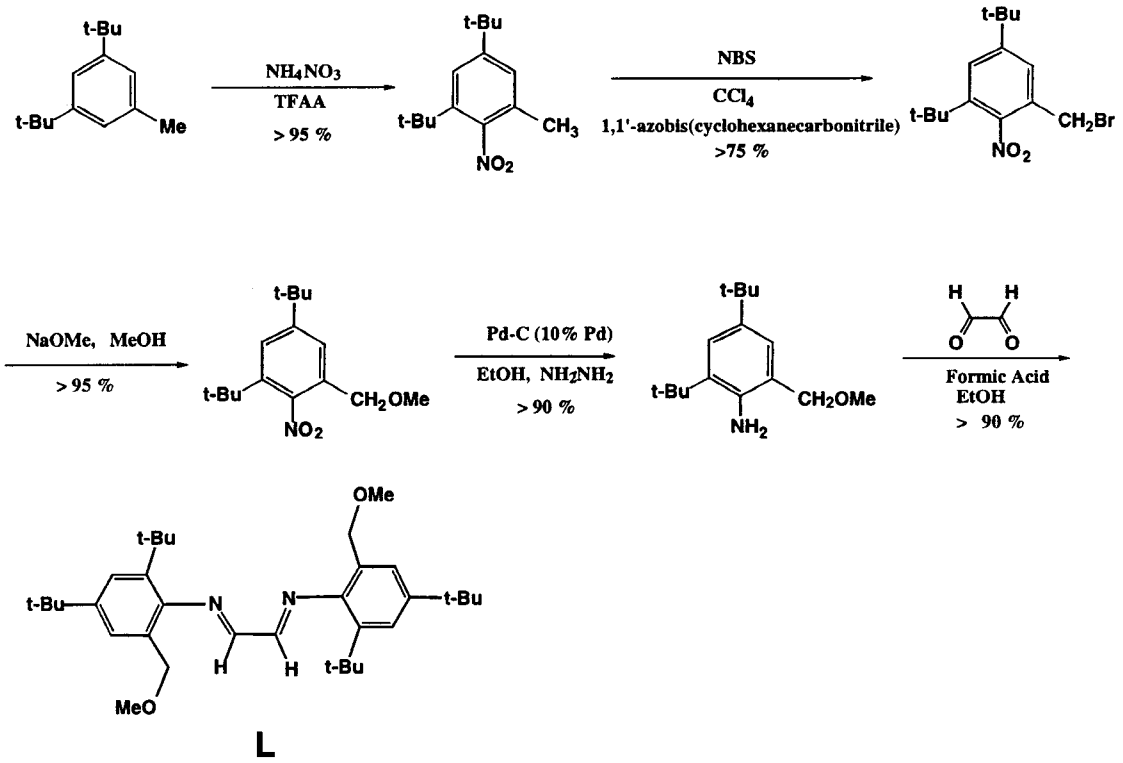

metal ion in the manner shown as **A** leaving two

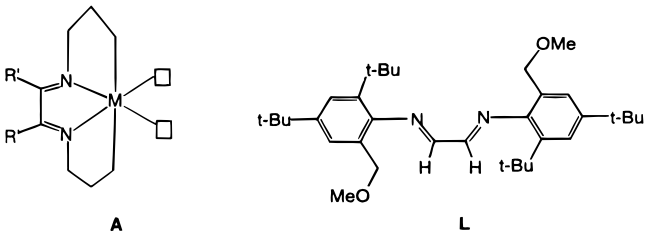

adjacent sites available for substrate binding and transformation in the manner of the Brookhart polymerization catalysts[1−9] and related Pd(II) catalysts studied by Drent for copolymerization of CO and ethylene.[24] In the design of the ligand, bulky organic substituents serve to enforce the desired geometric constraints while ensuring the solubility of the resultant complexes in nonpolar solvents. The specific DAB ligand initially designed in this exercise is shown as **L** where the two additional coordination sites are ether oxygens capable of weak but significant binding to metal ions. Studies by Dunbar on complexes of the functionalized phosphine $P(2,4,6\text{-}C_6H_2(OMe)_3)_3$ demonstrate the importance and versatility of coordination by the ortho methoxy ether substituents in stabilizing octahedral Rh(II) and Pd(II) ions.[25−27]

A second aspect in the design of **L** is that, for square-planar complexes similar to Brookhart's active catalysts,[1−9] two possible isomers for the M**L** moiety would exist—one having C_2 symmetry and the other with mirror symmetry—with possible stereochemical consequences in reactions promoted or catalyzed by it. Specifically, for the M**L** moiety of C_2 symmetry, diastereomeric interactions between the catalyst complex and prochiral substrates would exist. Additionally, the design of ligand **L** and related derivatives with other groups in place of methoxymethyl affords the possibility of developing catalysts in which secondary interactions between ligand and substrate help control the stereochemistry and course of the ensuing transformations.

Results and Discussion

Synthesis and Characterization of Ligands. The synthetic procedure for obtaining glyoxal bis(2-(methoxymethyl)-4,6-di-*tert*-butylphenyl)diimine (**L**) is outlined in Scheme 1, starting from commercially available 3,5-di-*tert*-butyltoluene. The details of each step leading to **L** can be found in the Experimental Section, and pertinent spectroscopic data for **L**, $\mathbf{LH_4}$, and all new complexes are summarized in Table 1.

The condensation reaction between 2-(methoxymethyl)-4,6-di-*tert*-butylaniline and glyoxal was initially examined under thermal conditions. Refluxing a 2:1 mixture of 2-(methoxymethyl)-4,6-di-*tert*-butylaniline and glyoxal in either methanol or ethanol solvents overnight produced only traces of the desired product as determined by monitoring the reactions with TLC analysis and ^{1}H NMR spectroscopy. Therefore, the thermal condensation route to **L** was not pursued further. Instead, the catalytic procedure used by tom Dieck and co-workers[28] for preparing similar 1,4-diazabutadiene ligands was employed. Treatment of a 2:1 mixture of 2-(methoxymethyl)-4,6-di-*tert*-butylaniline and glyoxal in minimum ethanol solvent with a catalytic amount of formic acid at room temperature affords **L** as an analytically pure yellow microcrystalline product in greater than 90% yield.

(24) Drent, E.; Budzelaar, P. H. M. *Chem. Rev.* **1996**, *96*, 663−681.
(25) Dunbar, K. R.; Sun, J.-S. *J. Chem. Soc., Chem. Commun.* **1994**, 2387−2388.
(26) Dunbar, K. R.; Haefner, S. C.; Pence, L. E. *J. Am. Chem. Soc.* **1989**, *111*, 5504−5506.
(27) Dunbar, K. R.; Matonic, J. H.; Saharan, V. P. *Inorg. Chem.* **1994**, *33*, 25−31.
(28) tom Dieck, H.; Svoboda, M.; Greiser, T. *Z. Naturforsch., B.: Anorg. Chem., Org. Chem.* **1981**, *36B*, 823.

Table 1. ^{1}H NMR Spectral Data for L, LH_4, and All New Complexes[a]

compd	^{1}H NMR (δ)
L	1.33 (s, 18H, *t*-Bu), 1.37 (s, 18H, *t*-Bu), 3.38 (s, 6H, OCH_3), 4.14 (s, 4H, CH_2), 7.28 (s, 2H, C_6H), 7.42 (s, 2H, C_6H), 8.19 (s, 2H, NCH)
LH_4	1.32 (s, 18H, *t*-Bu), 1.46 (s, 18H, *t*-Bu), 3.26 (s, 4H, NCH_2), 3.44 (s, 6H, OCH_3), 3.77 (s, 2H, NH), 4.57 (s, 4H, CH_2), 7.326 (s, 2H, C_6H), 7.331 (s, 2H, C_6H)
1a	1.32 (s, 18H, *t*-Bu), 1.59 (s, 18H, *t*-Bu), 336 (s, 6H, OCH_3), 4.29 (d, J_{HH} = 12 Hz, 2H, CH_aH), 5.29 (d, J_{HH} = 12 Hz, 2H, CHH_b), 7.18 (d, J_{HH} = 4 Hz, 2H, C_6H), 7.51 (d, J_{HH} = 4 Hz, 2H, C_6H, 7.96 (s, 2H, NCH)
1b	1.31 (s, 18H, *t*-Bu), 1.55 (s, 18H, *t*-Bu), 3.33 (s, 6H, OCH_3), 4.33 (d, J_{HH} = 12 Hz, 2H, CH_aH), 5.13 (d, J_{HH} = 12 Hz, 2H, CHH_b), 7.18 (d, J_{HH} = 4 Hz, 2H, C_6H), 7.47 (d, J_{HH} = 4 Hz, 2H, C_6H, 8.02 (s, 2H, NCH)
2a	1.36 (s, 18H, *t*-Bu), 1.54 (s, 18H, *t*-Bu), 3.31 (s, 6H, OCH_3), 4.33 (d, J_{HH} = 12 Hz, 2H, CH_aH), 5.16 (d, J_{HH} = 12 Hz, 2H, CHH_b), 7.57 (d, J_{HH} = 4 Hz, 2H, C_6H), 7.78 (d, J_{HH} = 4 Hz, 2H, C_6H, 8.73 (s, 2H, NCH)
2b	1.35 (s, 18H, *t*-Bu), 1.53 (s, 18H, *t*-Bu), 3.31 (s, 6H, OCH_3), 4.40 (d, J_{HH} = 12 Hz, 2H, CH_aH), 5.10 (d, J_{HH} = 12 Hz, 2H, CHH_b), 7.27 (d, J_{HH} = 4 Hz, 2H, C_6H), 7.55 (d, J_{HH} = 4 Hz, 2H, C_6H, 8.74 (s, 2H, NCH)
3	1.30 (s, 18H, *t*-Bu), 1.61 (s, 18H, *t*-Bu), 2.74 (m, 2H, NCHa), 3.66 (s, 6H, OCH_3), 3.26 (m, 2H, NCH_b), 4.68 (d, J_{HH} = 12 Hz, 2H, CH_aH), 6.09 (s, 2H, NH), 7.29 (s, 2H, C_6H), 7.38 (s, 2H, C_6H), 7.62 (d, J_{HH} = 12 Hz, 2H, CH_aH)
4	1.27 (s, 18H, *t*-Bu), 1.62 (s, 18H, *t*-Bu), 2.74 (m, 2H, NCHa), 3.61 (s, 6H, OCH_3), 3.74 (m, 2H, NCH_b), 4.64 (d, J_{HH} = 12 Hz, 2H, CH_aH), 7.28 (d, J_{HH} = 2 Hz, 2H, NH), 7.39 (d, J_{HH} = 2 Hz, 2H, C_6H), 7.66 (d, J_{HH} = 12 Hz, 2H, CHH_b),

[a] All ^{1}H NMR spectra were recorded in $CDCl_3$ solutions. Chemical shift values are reported in ppm. Abbreviations: s, singlet; d, doublet; m, multiplet.

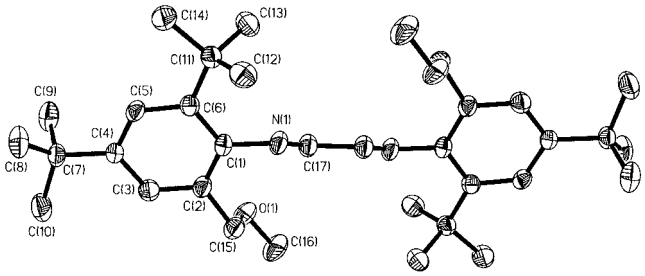

Figure 1. ORTEP diagram of **L**. Thermal ellipsoids are shown at 50% probability. Hydrogen atoms are omitted for clarity.

The ^{1}H NMR spectrum (Table 1) of **L** in $CDCl_3$ shows a characteristic imine proton resonance at δ 8.19 ppm as a sharp singlet,[10,28] along with singlets for the benzylic CH_2 protons at δ 4.14, the methoxy protons at δ 3.38, and the *tert*-butyl protons at δ 1.37 and 1.33 ppm. The fact that the diastereotopic benzylic protons show only a singlet instead of a four-line AB pattern indicates that free rotation about single bonds of the DAB backbone must be faster than the NMR time scale, despite the bulkiness of the ortho aryl substituents.[29,30] A single-crystal X-ray diffraction structure confirms the identity of **L** and reveals the preferred conformation of the free ligand. The ORTEP diagram of **L** is shown in Figure 1, with details of the structure determination, including unit-cell data, summarized in Table 2 and relevant bond distances, bond angles, and torsion angles listed in Tables 3−5, respectively.

As seen in Figure 1, **L** adopts a *trans* orientation at each imine functionality with an *s-trans* conformation about the central C−C bond of the DAB backbone. **L** contains a crystallographically imposed inversion center, and therefore the N═C−C═N DAB moiety is necessarily planar. The phenyl rings of the imine substituents are tilted out of the N═C−C═N plane by about 55°, as indicated by torsion angles of −128.19(0.24) and 57.14(0.31)° for C(17)−N(1)−C(1)−C(6) and C(17)−N(1)−C(1)−C(2), respectively. As a consequence of the crystallographically imposed symmetry, the methoxymethyl substituents are on opposite sides of the N═C−C═N plane. The bond distances for the C═N double bond and the central C−C single bond are 1.273(3) and 1.470(4) Å, respectively, which are similar to the bond distances described in other structurally characterized free diimine ligands.[10]

Glyoxal bis(2-(methoxymethyl)-4,6-di-*tert*-butylphenyl)diimine (**L**) can be reduced readily using $LiAlH_4$ as a reducing agent at room temperature. Treatment of a bright yellow THF solution of **L** with excess $LiAlH_4$ affords the saturated colorless product **LH_4** in high yield (eq 1). **LH_4** is very soluble in hexane, toluene, THF,

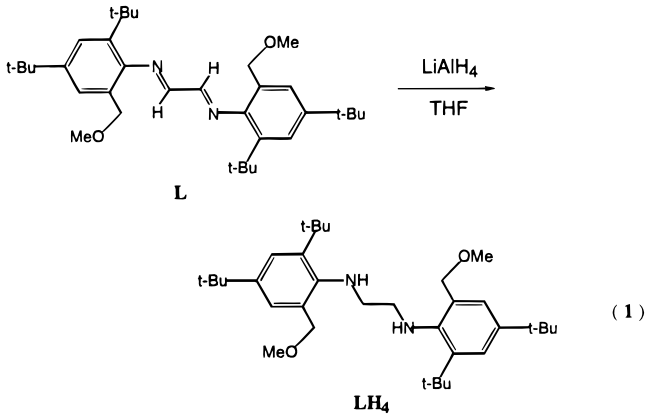

(1)

and CH_2Cl_2 and moderately soluble in CH_3OH and DMF. The ^{1}H NMR spectrum of **LH_4** (Table 1) in $CDCl_3$ shows resonances of secondary amine NH and NCH_2-CH_2N backbone protons at δ 3.77 and 3.26, along with those for the MeO protons at δ 3.44, the benzylic CH_2 protons at δ 4.57, and the *tert*-butyl groups at δ 1.32 and 1.46 ppm. The IR spectrum of **LH_4** in KBr reveals the NH stretches at 3422 and 3328 cm^{-1}.

Single crystals of **LH_4** were grown by slow evaporation from a methanol and hexane solution. The ORTEP diagram of **LH_4** is shown in Figure 2, with details of the structure determination, including unit-cell data, summarized in Table 2 and relevant bond distances, bond angles, and torsion angles listed in Tables 3−5, respectively.

(29) Wightman, R. H.; Staunton, J.; Battersby, A. R.; Hanson, K. R. *J. Chem. Soc., Perkin Trans. 1* **1972**, 2355.
(30) Jennings, B. *Chem. Rev.* **1975**, *75*, 307.

Table 2. Summary of Crystallographic Data and X-ray Experimental Details for L, LH_4, 2b, 3, and 4

	L	**LH_4**	**2b·CH_2Cl_2**
empirical formula	$C_{34}H_{52}N_2O_2$	$C_{34}H_{56}N_2O_2$	$C_{34}H_{54}Cl_4N_2O_2Pt$
fw	520.67	524.81	871.69
cryst syst	triclinic	monoclinic	monoclinic
space group	$P\bar{1}$ (No. 2)	$P2_1$ (No. 4)	$P2_1/c$ (No. 14)
Z	1	2	4
a, Å[a]	5.760(1)	5.9758(1)	16.9599(2)
b, Å	9.383(2)	17.4272(2)	18.4985(2)
c, Å	14.954(3)	15.6222(1)	12.4976(0)
α, deg	89.38(2)		
β, deg	79.67(2)	99.063(1)	100.945(0)
γ, deg	88.14(2)		
V, Å^3	794.7(3)	1606.61(3)	3849.58(6)
ρ_{calc}, g cm^{-3}	1.088	1.085	1.504
cryst dimens, mm	0.18 × 0.26 × 0.28	0.14 × 0.14 × 0.38	0.08 × 0.08 × 0.08
temp, °C	−80	−100	−90
radiation; λ, Å	Mo; 0.710 73	Mo; 0.710 73	Mo; 0.710 73
2θ range, deg	2−45	3−45	3−45
limiting indices	$-7 \le h \le 6$	$-7 \le h \le 7$	$-22 \le h \le 17$
	$-12 \le h \le 11$	$-23 \le h \le 11$	$-24 \le h \le 24$
	$-20 \le l \le 12$	$-20 \le l \le 20$	$-11 \le l \le 16$
no. of total data	4552	6506	14 525
no. unique data	1953	2976	4958
no. of obsd data	1559 ($I > 2\sigma(I)$)	2697 ($I > 2\sigma(I)$)	4237 ($I > 2\sigma(I)$)
agreement between equiv data	0.0219	0.0385	0.0342
no. of parameters varied	173	344	389
μ, mm^{-1}	0.066	0.066	3.954
abs cor	empirical (SADABS)	none	empirical (SADABS)
range of transm factors	0.695−0.928		0.795−0.928
$R_1(F_o)$, w$R_2(F_o^2)$ ($I > 2\sigma(I)$), %[b]	5.05, 12.27	4.90, 10.35	3.13, 6.05
$R_1(F_o)$, w$R_2(F_o^2)$ (all data), %	6.67, 13.36	5.66, 10.86	4.33, 6.56
goodness of fit[c]	1.065	1.094	1.049

	3·2CH_2Cl_2	**4**·2Me_2CO
empirical formula	$C_{36}H_{60}Cl_6N_2O_2Pd$	$C_{40}H_{68}Cl_2N_2O_4Pt$
fw	871.96	906.95
cryst syst	monoclinic	monoclinic
space group	$C2/c$ (No. 15)	$C2/c$ (No. 15)
Z	4	4
a, Å[a]	36.1506(8)	36.0649(3)
b, Å	8.0994(2)	8.1787(2)
c, Å	15.5671(1)	15.7585(3)
α, deg		
β, deg	113.988(1)	112.6100(1)
γ, deg		
V, Å^3	4164.3(1)	4290.9(1)
ρ_{calc}, g cm^{-3}	1.391	1.404
cryst dimens, mm	0.04 × 0.18 × 0.20	0.30 × 0.32 × 0.34
temp, °C	−90	−80
radiation; λ, Å	Mo; 0.710 73	Mo; 0.710 73
2θ range, deg	5−46.5	5−56.5
limiting indices	$-40 \le h \le 29$	$-46 \le h \le 47$
	$-8 \le h \le 7$	$-10 \le h \le 6$
	$-17 \le l \le 17$	$-20 \le l \le 18$
no. of total data	7930	12 954
no. unique data	2915	5067
no. of obsd data	2440 ($I > 2\sigma(I)$)	4868 ($I > 2\sigma(I)$)
agreement between equiv data	0.0485	0.0169
no. of parameters varied	216	205
μ, mm^{-1}	0.863	3.433
abs cor	empirical (SADABS)	empirical (SADABS)
range of transm factors	0.766−0.928	0.812−0.928
$R_1(F_o)$, w$R_2(F_o^2)$ ($I > 2\sigma(I)$), %[b]	5.65, 11.13	2.28, 5.49
$R_1(F_o)$, w$R_2(F_o^2)$ (all data), %	7.41, 11.90	2.44, 5.56
goodness of fit[c]	1.059	1.058

[a] It has been noted that the integration program SAINT produces cell constant errors that are unreasonably small, since systematic error is not included. More reasonable errors might be estimated at 10 times the listed values. [b] $R_1 = (\sum||F_o| - |F_c||)/\sum|F_o|$, w$R_2 = [\sum[w(F_o^2 - F_c^2)^2]/\sum[w(F_o^2)^2]]^{1/2}$, where $w = 1/[\sigma^2(F_o^2) + (aP)^2 + bP]$ and $P = [f(\text{maximum of 0 or } F_o^2) + 1 - f)F_c^2]$. [c] GOF $= S = [\sum[w(F_o^2 - F_c^2)^2]/(n - p)]^{1/2}$.

It is interesting to compare the structural features of **LH_4** and **L**. The direct consequence of the reduction is that the central N−C−C−N skeleton in **LH_4** is no longer planar, as shown by the torsion angle of 61.0(0.4)° about the N(1)−C(33)−C(34)−N(2) backbone. The longer C−N bond distances (1.468(5) Å for N(1)−C(33) and 1.465(5) Å for N(2)−C(34)) and the smaller C−C−N bond angles (110.5(3)° for N(1)−C(33)−C(34) and 109.6(3)° for N(2)−C(34)−C(33)) in **LH_4** are consistent with the change in the C and N hybridization from sp^2 in **L** to sp^3 in **LH_4** upon reduction. The orientation of the phenyl rings relative to the N−C−C−N backbone in **LH_4** is not as simple to describe as it is for **L**. Torsion angles of −101.00(0.40) and 78.38(0.43)° for C(33)−

Table 3. Selected Bond Distances (Å) for L, LH_4, 2b, 3, and 4

L			
O(1)−C(15)	1.423(3)	O(1)−C(16)	1.424(3)
N(1)−C(17)	1.273(3)	N(1)−C(1)	1.426(3)
C(2)−C(15)	1.512(3)	C(17)−C(17)′	1.470(4)
LH_4			
O(1)−C(7)	1.382(5)	O(1)−C(8)	1.423(5)
O(2)−C(24)	1.421(5)	O(2)−C(23)	1.430(5)
N(1)−C(1)	1.426(5)	N(1)−C(33)	1.468(5)
N(2)−C(17)	1.434(5)	N(2)−C(34)	1.465(5)
C(33)−C(34)	1.502(6)		
2b·CH_2Cl_2			
Pt−N(1)	1.990(4)	Pt−N(2)	2.017(4)
Pt−Cl(1)	2.2795(13)	Pt−Cl(2)	2.2835(14)
O(1)−C(8)	1.407(6)	O(1)−C(7)	1.411(6)
O(2)−C(24)	1.408(7)	O(2)−C(23)	1.427(7)
N(1)−C(33)	1.288(7)	N(2)−C(17)	1.455(6)
C(6)−C(7)	1.507(7)	C(22)−C(23)	1.516(7)
C(33)−C(34)	1.432(7)		
3·$2CH_2Cl_2$			
Pd−N(1)	2.089(4)	Pd−N(1)′	2.089(4)
Pd−Cl(1)	2.279(2)	Pd−Cl(1)′	2.279(2)
O(1)−C(7)	1.417(7)	O(1)−C(8)	1.435(7)
N(1)−C(1)	1.478(6)	N(1)−C(17)	1.505(7)
C(6)−C(7)	1.506(7)	C(17)−C(17)′	1.493(10)
4·$2Me_2CO$			
Pt−N(1)	2.093(2)	Pt−N(1)′	2.093(2)
Pd−Cl(1)	2.2955(6)	Pt−Cl(1)′	2.2955(6)
O(1)−C(7)	1.422(3)	O(1)−C(8)	1.428(3)
N(1)−C(1)	1.471(3)	N(1)−C(17)	1.503(3)
C(6)−C(7)	1.512(3)	C(17)−C(17)′	1.515(5)

Table 4. Selected Bond Angles (deg) for L, LH_4, 2b, 3, and 4

L			
C(15)−O(1)−C(16)	111.1(2)	C(17)−N(1)−C(1)	119.3(2)
C(2)−C(1)−C(6)	120.4(2)	C(6)−C(1)−N(1)	119.5(2)
O(1)−C(15)−C(2)	108.2(2)	N(1)−C(17)−C(17)′	118.9(3)
LH_4			
C(7)−O(1)−C(8)	112.2(4)	C(24)−O(2)−C(23)	111.9(3)
C(1)−N(1)−C(33)	114.7(3)	C(17)−N(2)−C(34)	118.1(3)
C(2)−C(1)−N(1)	122.7(4)	C(6)−C(1)−N(1)	118.5(3)
C(22)−C(17)−N(2)	120.0(3)	C(18)−C(17)−N(2)	120.3(4)
N(1)−C(33)−C(34)	110.5(3)	N(2)−C(34)−C(33)	109.6(3)
2b·CH_2Cl_2			
N(1)−Pt−N(2)	79.4(2)	N(1)−Pt−Cl(1)	94.08(13)
N(2)−Pt−Cl(1)	172.25(12)	N(1)−Pt−Cl(2)	173.60(13)
N(2)−Pt−Cl(2)	95.83(13)	Cl(1)−Pt−Cl(2)	90.95(5)
C(8)−O(1)−C(7)	111.2(4)	C(24)−O(2)−C(23)	112.1(4)
C(33)−N(1)−C(1)	118.0(5)	C(33)−N(1)−Pt	114.8(4)
C(1)−N(1)−Pt	127.1(3)	C(34)−N(2)−C(17)	117.3(4)
C(34)−N(2)−Pt	113.8(4)	C(17)−N(2)−Pt	127.0(3)
C(2)−C(1)−N(1)	124.2(5)	C(6)−C(1)−N(1)	114.2(5)
O(1)−C(7)−C(6)	109.8(4)	C(22)−C(17)−N(2)	114.2(5)
C(18)−C(17)−N(2)	123.3(5)	O(2)−C(23)−C(22)	113.4(4)
N(1)−C(33)−C(34)	115.8(5)	N(2)−C(34)−C(33)	116.1(5)
3·$2CH_2Cl_2$			
N(1)−Pd−N(1)′	83.2(2)	N(1)−Pd−Cl(1)	93.48(12)
N(1)′−Pd−Cl(1)	176.60(13)	N(1)−Pd−Cl(1)′	176.60(13)
N(1)′−Pd−Cl(1)′	93.47(13))	Cl(1)−Pd−Cl(1)′	89.89(9)
C(7)−O(1)−C(8)	111.3(5)	C(1)−N(1)−C(17)	112.9(4)
C(1)−N(1)−Pd	122.3(3)	C(17)−N(1)−Pd	107.3(3)
C(6)−C(1)−N(1)	119.0(5)	C(2)−C(1)−N(1)	119.8(5)
O(1)−C(7)−C(6)	111.3(4)	C(17)′−C(17)−N(1)	107.4(3)
4·$2Me_2CO$			
N(1)′−Pt−N(1)	82.95(11)	N(1)′−Pt−Cl(1)′	93.20(6)
N(1)−Pt−Cl(1)′	175.80(6)	N(1)′−Pt−Cl(1)	175.80(6)
N(1)−Pt−Cl(1)	93.20(6)	Cl(1)′−Pt−Cl(1)	90.70(3)
C(7)−O91)−C(8)	111.1(2)	C(1)−N(1)−C(17)	112.6(2)
C(1)−N(1)−Pt	122.3(2)	C(17)−N(1)−Pt	112.6(2)
C(1)−N(1)−Pt	122.3(2)	C(17)−N(1)−Pt	107.94(13)
C(6)−C(1)−N(1)	119.4(2)	C(2)−C(1)−N(1)	119.3(2)
O(1)−C(7)−C(6)	110.5(2)	N(1)−C(17)−C(17)′	107.3(2)

N(1)−C(1)−C(2) and C(33)−N(1)−C(1)−C(6) show that the phenyl rings, as in the structure of **L**, are largely rotated out of the average plane of the ethylenediamine backbone. As with the structure of **L**, the methoxymethyl substituents of the two aryl groups lie on opposite sides of the N−C−C−N average plane.

Synthesis and Characterization of $PdCl_2L$ (1a and 1b). The reaction between **L** and $Pd(PhCN)_2Cl_2$ proceeds rapidly in CH_2Cl_2 at room temperature to afford a 1:1 mixture of isomers **1a** and **1b**, as determined by TLC analysis and ^1H NMR spectroscopy. Compounds **1a** and **1b** are both very soluble in CH_2Cl_2, $CHCl_3$, and THF, moderately soluble in toluene, methanol, and ethanol, and insoluble in hydrocarbons. Both **1a** and **1b** are air stable in the solid state and in solution with no evidence of decomposition, even after exposure of the solutions to air for days.

The separation of **1a** and **1b** by fractional recrystallization proved to be unsuccessful due to similar solubilities of the two isomers in common organic solvents. However, a slight difference in polarity between **1a** and **1b**, arising from the *trans* and *cis* orientations of the methoxymethyl substituents, resulted in a small R_f differential (<0.1) on the TLC plates. This differential allowed for the successful separation of the isomers by preparative thin-layer chromatography using a mixture of CH_2Cl_2 and diethyl ether as eluant (30:1). The much lower yields of **1a** and **1b** after separation by TLC stemmed from slow decomposition over the long separation times needed on the thin-layer plates.

Compounds **1a** and **1b** have very similar ^1H NMR spectra in $CDCl_3$. A characteristic feature of the ^1H spectra for **1a** and **1b** is the diastereotopic nature of the benzylic protons which appear as two sets of doublets centered at δ 5.28 and 4.29 for **1a** and at δ 5.12 and 4.33 for **1b**, with the same J_{HH} coupling constant of 12 Hz for each set. The benzylic protons for both isomers thus exhibit an AB coupling pattern similar to that seen for other geometrically rigid benzylic systems.[30−32] Irradiation of either set of the two doublets of benzylic protons results in a sharp singlet for the second set, a fact that corroborates the diastereotopic nature of the two protons attached to the benzylic carbon atom. Compared to those of the free ligand **L**, the diimine proton resonances for **1a** and **1b** are shifted to higher field by ~0.2 ppm.

Rotations around the C_{aryl}−N and central C−C bonds in free ligand **L** need to be considered in order to explain the formation of the two isomers. As discussed previously, both rotations in the free ligand are fast on the NMR time scale, as indicated by the single benzyl proton resonance in the ^1H NMR spectrum of **L**. While rotation of the central C−C bond is responsible for the change in conformation of the N=C−C=N backbone from *s-trans* in **L** to *s-cis* in **1a** and **1b**, rotation about the C_{aryl}−N bond determines the orientation of the $MeOCH_2$− substituents relative to the coordination plane. The successful separation of isomers **1a** and **1b** indicates that rotation about the C_{aryl}−N bonds is effectively hindered upon coordination as a consequence of steric repulsions between the aryl ring substituents and the metal−diimine chelate ring.

Synthesis and Characterization of $LPtCl_2$ (2a and 2b). The reaction between **L** and $Pt(PhCN)_2Cl_2$

(31) Atwood, D. A.; Jegier, J. A.; Martin, K. J.; Rutherford, D. *Organometallics* **1995**, *14*, 1453−1460.
(32) Atwood, D. A.; Remington, M. P.; Rutherford, D. *Organometallics* **1996**, *15*, 4763−4769.

Table 5. Selected Torsion Angles (deg) for L, LH_4, 2b, 3, and 4

L	
C(17)−N(1)−C(1)−C(6)	−128.19(0.24)
C(17)−N(1)−C(1)−C(2)	57.14(0.31)
N(1)−C(17)−C(17)′−N(1)′	180.00(0)
N(1)−C(1)−C(2)−C(15)	−3.61(0.34)
N(1)−C(1)−C(2)−C(11)	1.46(0.32)
C(1)−C(2)−C(15)−O(1)	−92.44(0.26)
C(1)−N(1)−C(17)−C(17)	−175.71(.26)
LH_4	
N(1)−C(33)−C(34)−N(2)	60.96(0.42)
C(1)−N(1)−C(33)−C(34)	−169.46(0.33)
C(17)−N(2)−C(34)−C(33)	−178.38(0.34)
C(33)−N(1)−C(1)−C(2)	−101.00(0.42)
C(33)−N(1)−C(1)−C(6)	78.38(0.43)
C(1)−C(6)−C(7)−O(1)	173.77(0.39)
N(1)−C(1)−C(6)−C(7)	7.55(0.56)
N(1)−C(1)−C(2)−C(9)	−11.54(0.57)
N(2)−C(17)−C(18)−C(29)	−0.46(0.54)
N(2)−C(17)−C(22)−C(23)	−2.29(0.55)
C(17)−C(22)−C(23)−O(2)	−97.28(0.44)
2b·CH_2Cl_2	
N(1)−C(33)−C(34)−N(2)	2.72(0.73)
Pt−N(2)−C(34)−C(33)	−0.77(0.59)
Pt−N(1)−C(33)−C(34)	−3.28(0.61)
C(1)−N(1)−C(33)−C(34)	172.57(0.44)
C(17)−N(2)−C(34)−C(33)	−166.19(0.44)
C(33)−N(1)−C(1)−C(2)	90.64(0.66)
C(33)−N(1)−C(1)−C(6)	−88.19(0.60)
C(34)−N(2)−C(17)−C(18)	94.94(0.66)
C(34)−N(2)−C(17)−C(22)	82.91(0.61)
N(2)−C(17)−C(18)−C(29)	−5.20(0.93)
N(2)−C(17)−C(22)−C(23)	3.18(0.76)
C(17)−C(22)−C(23)−O(2)	−71.43(0.67)
C(1)−C(6)−C(7)−O(1)	179.23(0.48)
Pt−N(1)−C(1)−C(2)	−94.08(0.58)
Pt−N(1)−C(1)−C(6)	87.08(0.53)
Pt−N(2)−C(17)−C(18)	101.83(0.55)
Pt−N(2)−C(17)−C(22)	−80.32(0.58)
Cl(1)−Pt−N(1)−C(1)	2.55(0.42)
Cl(2)−Pt−N(1)−C(1)	144.17(0.97)
Cl(1)−Pt−N(1)−C(33)	177.96(0.37)
Cl(2)−Pt−N(1)−C(33)	−40.43(1.38)
Cl(1)−Pt−N(2)−C(17)	163.02(0.43)
Cl(2)−Pt−N(2)−C(17)	−21.34(0.41)
Cl(1)−Pt−N(2)−C(34)	−34.11(1.14)
Cl(2)−Pt−N(2)−C(34)	174.93(0.35)
3·2CH_2Cl_2	
N(1)−C(17)−C(17)′−N(1)′	58.14(0.73)
N(1)−C(1)−C(6)−C(7)	−174.81(0.50)
C(1)−C(6)−C(7)−O(1)	−90.85(0.64)
N(1)−C(1)−C(2)−C(9)	−4.70(0.79)
Pd−N(1)−C(17)−C(17)′	−43.31(0.53)
C(1)−N(1)−C(17)−C(17)′	−179.03(0.46)
Cl(1)′−Pd−N(1)−C(1)	157.22(2.18)
Cl(1)′−Pd−N(1)−C(17)	24.40(2.65)
Cl(1)−Pd−N(1)−C(17)	24.40(2.65)
Cl(1)−Pd−N(1)−C(1)	−31.49(0.39)
Pd−N(1)−C(1)−C(2)	121.29(0.46)
Pd−N(1)−C(1)−C(6)	−59.66(0.60)
4·2Me_2CO	
N(1)−C(17)−C(17)′−N(1)′	57.02(0.34)
N(1)−C(1)−C(6)−C(7)	5.41(0.37)
C(1)−C(6)−C(7)−O(1)	−91.47(0.27)
N(1)−C(1)−C(2)−C(9)	−3.72(0.36)
Pt−N(1)−C(17)−C(17)′	−42.71(0.25)
C(1)−N(1)−C(17)−C(17)′	179.39(0.22)
Cl(1)−Pt−N(1)−C(17)	−163.14(0.14)
Cl(1)−Pt−N(1)−C(1)	−31.49(0.39)
Pt−N(1)−C(1)−C(6)	71.25(0.28)
Pt−N(1)−C(1)−C(2)	121.09(0.21)
C(17)−N(1)−C(1)−C(2)	−107.88(0.25)
C(17)−N(1)−C(1)−C(6)	71.25(0.28)

was performed initially in CH_2Cl_2 at room temperature, corresponding to conditions used for the preparation of **1a** and **1b**. However, no reaction was observed after stirring the reaction mixture overnight. In contrast,

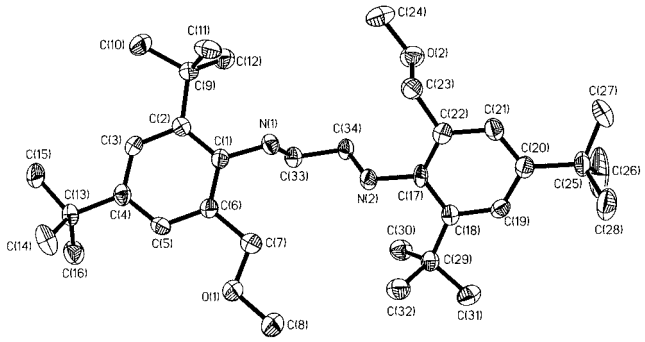

Figure 2. ORTEP diagram of LH_4. Thermal ellipsoids are shown at 50% probability. Hydrogen atoms are omitted for clarity.

refluxing in chloroform or toluene gave the desired isomeric products **2a** and **2b** after several hours, as depicted in eq 2.

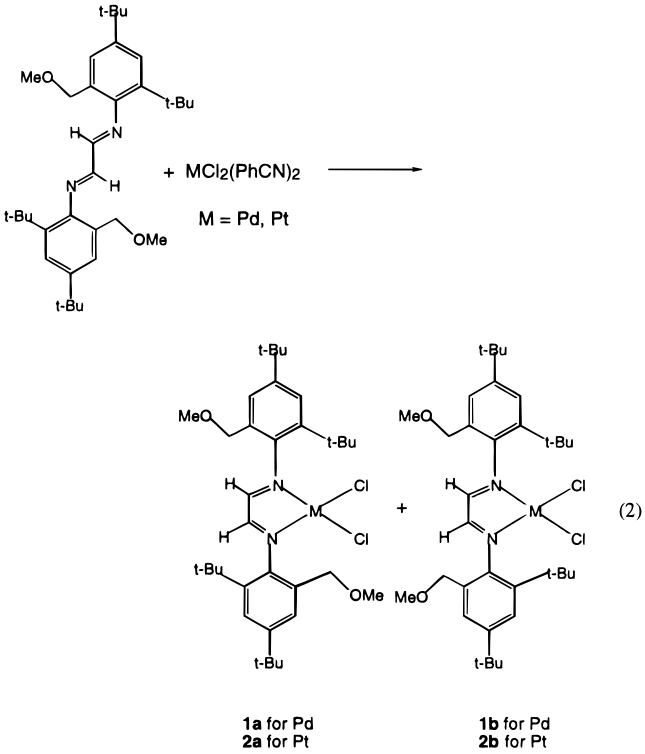

The physical properties of isomers **2a** and **2b** are very similar to those of **1a** and **1b**. The separation of **2a** and **2b**, however, is easier than for **1a** and **1b**, as the R_f differential for the former pair is larger than that for the latter. The lower yields for the formation of **2a** and **2b** also arise from the slow decomposition of the isomers during TLC separations.

Compounds **2a** and **2b** give very similar ^{1}H NMR spectra in $CDCl_3$ relative to those of the Pd analogs **1a** and **1b.** The diastereotopic protons for the benzylic CH_2 groups appear as two doublets centered at δ 5.15 and 4.33 for **2a** and at δ 5.10 and 4.40 for **2b**, with the same coupling constant of J_{HH} = 12 Hz. An observable difference between the NMR spectra for the Pd and Pt complexes **1** and **2** is observed in the chemical shifts of the imine protons. Compared to those of the free ligand **L**, the imine proton resonances for both **2a** and **2b** are shifted downfield about 0.5 ppm; these shifts are opposite to those observed for **1a** and **1b**. The reason for these differences is not fully understood.

X-ray Structure of $LPtCl_2$ (2b). Attempts to obtain X-ray-quality single crystals of compounds **1a**, **1b**, and **2a** from a variety of solvents under various conditions were not successful. Conversely, single crystals of **2b** as a methylene chloride solvate were grown from a mixture of CH_2Cl_2 and hexane solution at room temperature. The ORTEP diagram of **2b** is shown in Figure 3, with details of the structure determination, including unit-cell data, summarized in Table 2 and relevant bond distances, bond angles, and torsion angles listed in Tables 3−5, respectively.

As shown in Figure 3, complex **2b** is a distorted square-planar complex. The bond angles deviate from the idealized 90° value by virtue of the constraints imposed by chelation of **L**. This distortion is illustrated by the N(1)−Pt−N(2) bond angle of 79.4(2)°. The metal-chelate ring in **2b** is almost flat as indicated by the torsion angels of 2.72(0.73), −0.77(0.59), and −3.28-(0.61)° for N(1)−C(33)−C(34)−N(2), Pt−N(2)−C(34)−C(33), and Pt−N(2)−C(33)−C(34), respectively. The aryl rings lie nearly perpendicular to the metal-chelate ring as shown by the torsion angles of 90.64(0.66), −88.19(0.60), 94.94(0.66), and 82.91(0.61)°, respectively, for C(33)−N(1)−C(1)−C(2), C(33)−N(1)−C(1)−C(6), C(34)−N(2)−C(17)−C(18), and C(34)−N(2)−C(17)−C(22). These torsion angles are greater by nearly 20° than the corresponding values for the free ligand **L** and may be caused by greater steric repulsions in the chelated complex. The diffraction study also reveals the relative orientation of the two CH_2OMe groups in **2b** as *cisoid*, that is, on the same side of the coordination plane. The bond distances and bond angles for **2b** are very similar to those of other reported square-planar platinum diimine complexes.[16,33]

Synthesis and Characterization of $PdCl_2(LH_4)$ (3). The saturated ligand $\mathbf{LH_4}$ reacts readily with $Pd(PhCN)_2Cl_2$ in CH_2Cl_2 at room temperature to give compound **3** in almost quantitative yield (eq 3). The

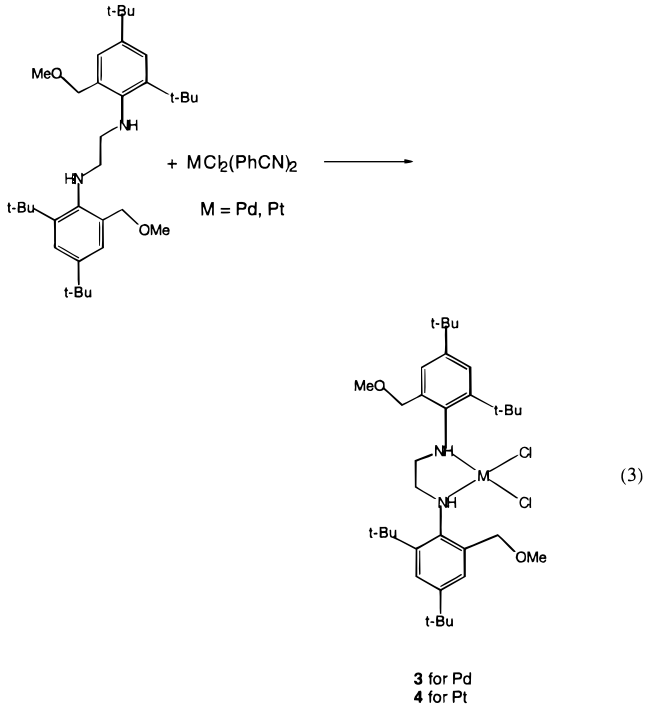

(3)

^1H NMR spectrum of **3** in $CDCl_3$ shows resonances of the *tert*-butyl groups at δ 1.30 and 1.61 and the methoxy protons at δ 3.36 as sharp singlets. As seen in **1** and **2**,

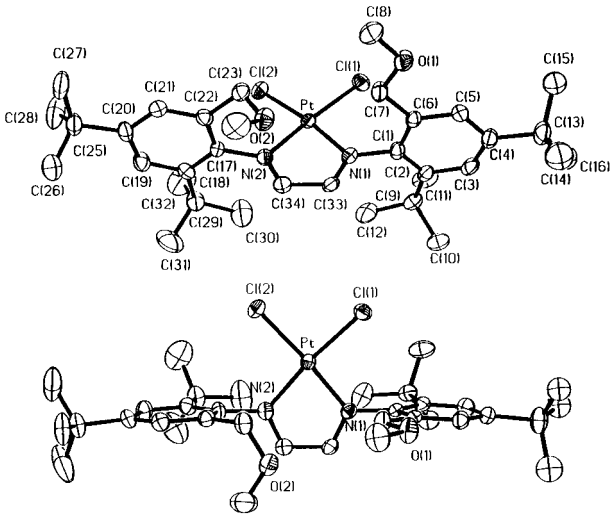

Figure 3. ORTEP diagrams of $\mathbf{LPtCl_2}$ (**2b**). Thermal ellipsoids are shown at 50% probability. Hydrogen atoms are omitted for clarity.

the benzylic CH_2 protons are diastereotopic in **3**, but unlike **1** and **2**, the relative chemical shifts are quite different with two doublets at δ 7.62 and 4.62, both having coupling constants of J_{HH} = 12 Hz. The methylene protons of the NCH_2CH_2N backbone are also diastereotopic, exhibiting two sets of multiplets at δ 2.70 and 3.74. The assignments of the NMR data were confirmed by proton homonuclear decoupling experiments. Irradiating each set of doublets at δ 7.62 and 4.62 results in the decoupling of the second set which coalesces to a sharp singlet. Similar experiments were performed for the protons of the NCH_2CH_2N backbone, irradiating the multiplets at either δ 3.74 or δ 2.70. The NH protons are seen at δ 6.09 as a broad resonance. The large observed chemical shift difference for the two diastereotopic benzyl protons in **3** is unusual and may be rationalized by the nature of the central NCH_2CH_2N backbone associated with **3** and the resulting conformational effects involving the metal-chelate ring (*vide infra*). The IR spectrum of **3** reveals NH stretches at 3363 and 3320 cm^{-1}.

Synthesis and Characterization of $PtCl_2(LH_4)$ (4). The reaction between the saturated ligand $\mathbf{LH_4}$ and $Pt(PhCN)_2Cl_2$, in either refluxing dichloromethane or chloroform, affords compound **4** in >60% yield (eq 3). Purification was achieved by recrystallization of the crude material from a mixture of acetone and hexane (1:3) to give **4** as large yellow plates. Attempted separation of **4** by column chromatography was not successful because of decomposition.

Compound **4** shows properties very similar to those of **3**. The ^1H NMR spectrum of **4** in $CDCl_3$ reveals a spectrum almost identical to that of **3** with proton resonances of the *tert*-butyl groups at δ 1.34 and 1.65 and the methoxy protons at δ 3.64, all as single sharp singlets. The diastereotopic benzyl protons are observed as two doublets centered at δ 4.66 and 7.68 with J_{HH} of 12 Hz. The methylene protons of the $NHCH_2CH_2NH$ backbone appear as two sets of multiplets centered at δ 2.80 and 3.89, while the NH protons are seen at δ 5.68 as a broad resonance. As with **3**, the assignment of the NMR data for **4** was confirmed by proton homonuclear

(33) van der Poel, H.; van Koten, G.; Kokkes, M.; Stam, C. H. *Inorg. Chem.* **1981**, *20*, 2941−2956.

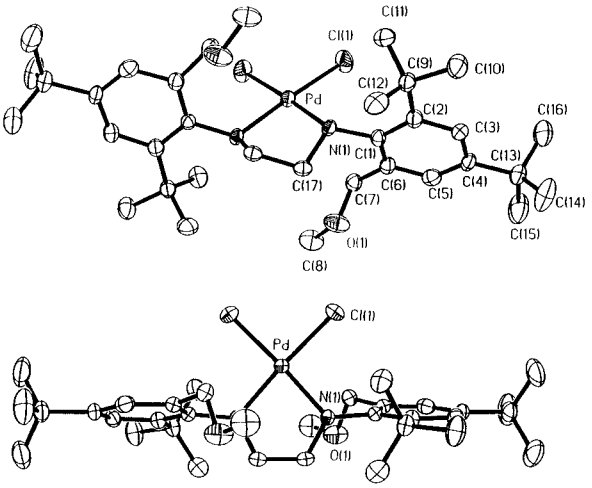

Figure 4. ORTEP diagrams of $\mathbf{PdCl_2(LH_4)}$ (**3**). Thermal ellipsoids are shown at 50% probability. Hydrogen atoms are omitted for clarity.

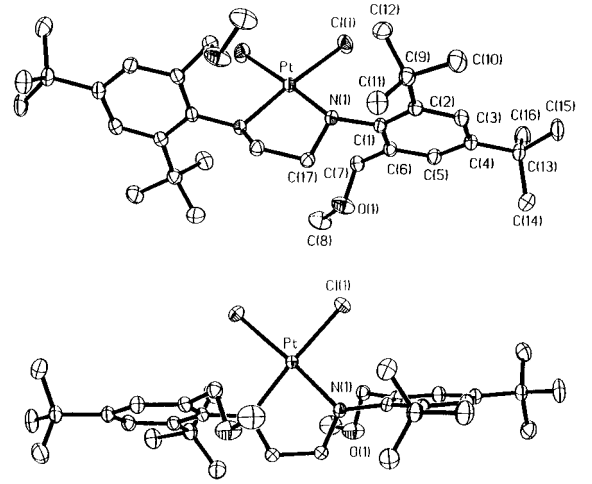

Figure 5. ORTEP diagrams of $\mathbf{PtCl_2(LH_4)}$ (**4**). Thermal ellipsoids are shown at 50% probability. Hydrogen atoms are omitted for clarity.

decoupling experiments. The IR spectrum shows the NH stretches for **4** at 3353 and 3317 cm^{-1}.

X-ray Structures of $\mathbf{PdCl_2(LH_4)}$ (3) and $\mathbf{PtCl_2(LH_4)}$ (4). Structures of **3** and **4** were determined by single-crystal X-ray diffraction. Crystals of **3** were grown from a saturated CH_2Cl_2/hexane solution, while crystals of **4** were obtained from a saturated acetone/hexane solution. The Pd complex **3** crystallizes as a methylene chloride solvate, while the isostructural Pt analog **4** forms as an acetone solvate. Figures 4 and 5 show ORTEP diagrams of **3** and **4**, and details of the structure determinations are summarized in Table 2. Relevant bond distances, bond angles, and torsion angles for the two structures are listed in Tables 3−5, respectively.

The structural features of **3** and **4** are strikingly similar. In contrast with that of **2**, the metal-chelate rings of **3** and **4** are distinctly nonplanar with N(1)−C(17)−C(17)′−N(1)′ torsion angles of 58.1(0.7) and 57.0(0.3)°, respectively. The conformation of the metal-chelate ring also causes the two protons on each methylene of the ethylenediamine backbone to be inequivalent, occupying pseudoaxial and pseudoequatorial positions with respect to the chelate ring. The NMR data indicate that these protons do not interconvert on the NMR time scale owing to the large steric interactions that exist between the backbone and the aryl ring substituents. As seen in the structure of **2b**, the aryl rings in **3** and **4** are rotated out of the coordination plane of the square-planar M(II) ions. Compared to the case of the free ligand $\mathbf{LH_4}$, the coordination of $\mathbf{LH_4}$ to the MCl_2 fragments in **3** and **4** also results in longer bond distances for the C(17)−N(1) (1.507(7) Å for **3**, 1.503(3) Å for **4**) and the C(17)−C(17)′ (1.496(1) Å for **3**, 1.515-(5) Å for **4**) bonds.

Conclusions

The synthesis and characterization of a new DAB ligand, glyoxal bis(2-(methoxymethyl)-4,6-(di-*tert*-butyl)-phenyl)diimine (**L**), and its reduced analog ($\mathbf{LH_4}$) have been demonstrated. The synthetic procedure for preparing **L**, as shown in Scheme 1, offers great versatility for the generation of other potentially tetradentate ligands as well as novel bidentate ligands for complexes of possible catalytic interest. With regard to the former, replacement of the MeO groups in **L** by other functional moieties such as R_2N, R_2P, and SR can in principle be accomplished easily, thereby generating a variety of N_4, N_2P_2, and N_2S_2 ligands with different binding properties.[34−36] The facile reduction of **L** to $\mathbf{LH_4}$ provides a direct comparison of unsaturated and saturated ligands for their coordinating abilities to metal ions. Furthermore, the unsaturated $\mathbf{LH_4}$ may be easily deprotonated to afford diamides $\mathbf{LH_2^{2-}}$ that are also capable of forming metal complexes by nitrogen coordination to higher valent metal ions.

The bidentate complexation of **L** and $\mathbf{LH_4}$ through the N donors for Pt(II) and Pd(II) has been investigated. The metal centers in compounds **1a**, **1b**, **2a**, **2b**, **3**, and **4** possess square-planar coordination geometries with the aryl groups of the **L** and $\mathbf{LH_4}$ ligands oriented out of the coordination plane in a manner that inhibits access to possible axial ligation sites. The formation of two isomers with *cis* and *trans* $MeOCH_2-$ groups indicates hindered rotation about the aryl C−N bond resulting from the steric bulkiness of the methoxymethyl and *tert*-butyl groups. The diastereotopic nature of the benzylic protons, especially for **3** and **4**, is consistent with this view and resultant conformational effects for the diimine (N=CHCH=N) and diamine ($NHCH_2CH_2NH$) metal-chelate rings.

Efforts to generate alkyl derivatives $MR_2\mathbf{L}$, $MR_2\mathbf{LH_4}$, and related cationic complexes from **1a**, **1b**, **2a**, **2b**, **3**, and **4** and study their potential catalytic activity with various substrates are in progress. Investigation of the possible interactions of methoxy groups of **L** and $\mathbf{LH_4}$ with d^6 metal centers in cationic complexes is also being pursued and will be reported in due course.

Experimental Section

Procedures and Materials. Glyoxal (40% in water), 3,5-di-*tert*-butyltoluene, hydrazine hydrate ($NH_2NH_2{\cdot}H_2O$, 98%), Pd−C (10% Pd), $LiAlH_4$, trifluoroacetic anhydride (TFAA), 1,1′-azobis(cyclohexanecarbonitrile), NaOMe (powder, 95%), and *N*-bromosuccinimide (NBS) were purchased from Aldrich Chemical Co. The complexes $PdCl_2(PhCN)_2$ and $PtCl_2(PhCN)_2$

(34) Anderson, D. J.; Eisenberg, R. *Organometallics* **1996**, *15*, 1697−1706.
(35) Mak, S.-T.; Yam, V. W.-W.; Che, C.-M.; Mak, T. C. W. *J. Chem. Soc., Dalton Trans.* **1990**, 2555−2564.
(36) Zheng, Y. Y.; Saluja, S.; Yap, G. P. A.; Blumenstein, M.; Rheingold, A. L.; Francesconi, L. C. *Inorg. Chem.* **1996**, *35*, 6656−6666.

were synthesized according to published procedures.[37,38] CH_2Cl_2 and CCl_4 were distilled from CaH_2 while THF and toluene were distilled from sodium/benzophenone ketyl radical freshly before use. All deuterated solvents were dried with appropriate drying agents, vacuum-transferred into Schlenk storage vessels, and stored under nitrogen.

Unless otherwise noted, all reactions and manipulations were performed in dry glassware under a nitrogen atmosphere using either standard Schlenk techniques or an inert-atmosphere glovebox. All NMR spectra were recorded on a Bruker AMX 400 MHz spectrometer. Proton homonuclear decoupling experiments were performed using the pulse program HOMODEC. IR spectra were recorded on a 6020 Galaxy series FT-IR spectrometer. Elemental analyses were obtained from Desert Analytics, Tucson, AZ.

Synthesis of the Glyoxal Bis(2-(methoxymethyl)-4,6-di-*tert*-butylphenyl)imine (L). The synthetic procedure leading to **L**, starting from 3,5-di-*tert*-butyltoluene, is outlined in Scheme 1 with the experimental details for each step documented below.

2-Nitro-3,5-di-*tert*-butyltoluene.[39] A 50 mL round-bottom flask was charged with 4.0 g (19.6 mmol) of 3,5-di-*tert*-butyltoluene, 1.6 g (20 mmol) of ammonium nitrate, and 15 mL of trifluoroacetic anhydride (TFAA). The reaction mixture was stirred at room temperature for 3 h, during which ammonium nitrate gradually dissolved and the color of the mixture changed from colorless to yellow brown. The reaction mixture was slowly poured into 150 mL of distilled water, and the resultant cream-colored solid mass was collected by filtration. The solid was thoroughly washed with water and then air-dried. Recrystallization of the crude material from hot methanol afforded nearly colorless crystals. Yield: 4.7 g (95%). ^{1}H NMR ($CDCl_3$): δ 1.29 (s, 9H, *t*-Bu), 1.36 (s, 9H, *t*-Bu), 2.21 (s, 3H, CH_3), 7.11 (s, 1H, C_6H), 7.35 (s, 1H, C_6H).

2-Nitro-3,5-di-*tert*-butyl-α-bromotoluene. To a 250 mL Schlenk flask were added 4.0 g (16 mmol) of 2-nitro-3,5-di-*tert*-butyltoluene, 3.2 g (18 mmol) of N-bromosuccinimide (NBS), 0.50 g of 1,1′-azobis(cyclohexanecarbonitrile), and 150 mL of carbon tetrachloride. This mixture was heated to reflux for 10 h and then cooled to room temperature (the reaction mixture at this point showed about 60−70% of the bromination product along with unreacted starting material; however, increasing the amount of NBS to 1.5 equiv and extending the reaction time led to no improvement in the extent of reaction). The white precipitate (succinamide) was removed by filtration, and the filtrate was rotaevaporated to dryness. The filtrate residue was then passed through a short silica gel column using a mixture of CH_2Cl_2 and hexanes (1:1) to remove any remaining succinamide and decomposed material. The mixture of 2-nitro-3,5-di-*tert*-butyltoluene and 2-nitro-3,5-di-*tert*-butyl-α-bromotoluene was treated with excess NaOMe in refluxing methanol to convert the bromide to methoxide (vide infra). The bromination product was characterized by ^{1}H NMR spectroscopy. ^{1}H NMR ($CDCl_3$): δ 1.29 (s, 9H, *t*-Bu), 1.36 (s, 9H, *t*-Bu), 4.40 (s, 2H, CH_2), 7.40 (s, 1H, C_6H), 7.60 (s, 1H, C_6H).

2-Nitro-3,5-di-*tert*-butyl-α-methoxytoluene. To a 250 mL Schlenk flask containing 150 mL of degassed methanol was added 6.0 g of the mixture of 2-nitro-3,5-di-*tert*-butyltoluene and 2-nitro-3,5-di-*tert*-butyl-α-bromotoluene (4:6) and 2.5 g of NaOMe (excess). This mixture was heated to reflux, and the reaction was monitored by TLC analysis until no 2-nitro-3,5-di-*tert*-butyl-α-bromotoluene remained present in the reaction solution (3−6 h). After the solution was cooled to room temperature, the solvent was removed using a rotary evaporator. The residue was dissolved in hexanes and purified by column chromatography on silica gel using a mixture of CH_2Cl_2 and hexanes (1:1) as eluant. Yield: 3.5 g. ^{1}H NMR ($CDCl_3$): δ 1.32 (s, 9H, *t*-Bu), 1.37 (s, 9H, *t*-Bu), 3.36 (s, 3H, OCH_3), 4.33 (s, 2H, CH), 7.26 (d, 1H, J_{HH} = 4 Hz, C_6H_2), 7.35 (d, 1H, J_{HH} = 4 Hz, C_6H_2).

2-(Methoxymethyl)-4,6-di-*tert*-butylaniline. A 250 mL Schlenk flask containing 150 mL of degassed ethanol was charged with 1.5 g (5.4 mmol) of 2-nitro-3,5-di-*tert*-butyl-α-methoxytoluene, 0.4 g of Pd−C catalyst (10% Pd), and 5.0 mL of $NH_2NH_2{\cdot}H_2O$. The above mixture was heated to reflux, and reaction was monitored by TLC analysis until no 2-nitro-3,5-di-*tert*-butyl-α-methoxytoluene was seen (12 h). After the reaction mixture was cooled to room temperature, the Pd−C catalyst was removed by filtration and the product was separated by column chromatography on silica gel. A trace of the starting material was eluted first with 1:1 mixture of CH_2Cl_2 and hexanes, and the product was eluted with pure CH_2Cl_2. Yield: 1.26 g (95%). ^{1}H NMR ($CDCl_3$): δ 1.29 (s, 9H, *t*-Bu), 1.44 (s, 9H, *t*-Bu), 3.37 (s, 3H, OCH_3), 4.32 (s, 2H, NH_2), 4.48 (s, 2H, CH_2), 6.98 (d, 1H, J_{HH} = 2.4 Hz, C_6H), 7.24 (d, 1H, J_{HH} = 2.4 Hz, C_6H).

Glyoxal Bis(2-(methoxymethyl)-4,6-di-*tert*-butylphenyl)imine (L). A 25 mL round-bottom flask containing 5 mL of absolute ethanol was charged with 0.80 g (3.2 mmol) of 2-(α-methoxymethyl)-4,6-di-*tert*-butylaniline, 0.18 mL of glyoxal (1.6 mmol, 40% in water), and a few drops of formic acid as catalyst. The color of the mixture turned from colorless to yellow immediately, and a yellow precipitate appeared after 5 min. The reaction mixture was stirred for an additional day, and the yellow solid was collected by filtration and washed with cold methanol to afford the analytically pure ligand. Additional crops of product may be obtained by drying the filtrate and chromatographing the residue on silica gel using CH_2Cl_2 as the solvent. Yield: 0.75 g (90%). ^{1}H NMR ($CDCl_3$): δ 1.33 (s, 18H, *t*-Bu), 1.37 (s, 18H, *t*-Bu), 3.38 (s, 6H, OCH_3), 4.14 (s, 4H, CH_2), 7.28 (s, 2H, C_6H), 7.42 (s, 2H, C_6H), 8.19 (s, 2H, NCH). Anal. Calcd for $C_{34}H_{52}O_2N_2$: C, 78.41; H, 10.06; N, 5.38. Found: C, 78.58; H, 10.29; N, 5.35.

LH_4. A 50 mL Schlenk flask containing 20 mL of THF was charged with 0.6 g (1.15 mmol) of glyoxal bis(2-(methoxymethyl)-4,6-di-*tert*-butylphenyl)imine (L), to which 6.0 mL of 1 M $LiAlH_4$ solution in THF was added dropwise by syringe. The yellow color of the solution diminished quickly upon addition of the $LiAlH_4$, and the reaction mixture was stirred for an additional 1 h. With caution, 5 mL of methanol was added slowly by syringe to destroy the excess $LiAlH_4$, and the resultant mixture was dried using the rotary evaporator. The purification of LH_4 was achieved by passing the crude product through a short silica gel or alumina column using a mixture of CH_2Cl_2 and ethanol (9:1). Alternatively, the product may be extracted with hexane from the crude material and then recrystallized from hot methanol. Yield: 0.57 g (90%). ^{1}H NMR ($CDCl_3$): δ 1.32 (s, 18H, *t*-Bu), 1.46 (s, 18H, *t*-Bu), 3.26 (s, 4H, NCH_2), 3.44 (s, 6H, OCH_3), 3.77 (s, 2H, NH), 4.57 (s, 4H, CH_2), 7.326 (s, 2H, C_6H), 7.331 (s, 2H, C_6H). IR (KBr): 3422 (w), 3328 (w) cm^{-1}. Anal. Calcd for $C_{34}H_{56}O_2N_2$: C, 77.81; H, 10.76; N, 5.34. Found: C, 77.79; H, 10.97; N, 5.30.

Synthesis of $LPdCl_2$ (1a and 1b). To a 50 mL Schlenk flask containing 10 mL of CH_2Cl_2 were added with 0.05 g (0.096 mmol) of glyoxal bis(2-(methoxymethyl)-4,6-di-*tert*-butylphenyl)imine (L) and 0.037 g (0.096 mmol) of $PdCl_2(PhCN)_2$, after which the reaction solution was stirred for 2 h. TLC analysis showed the disappearance of the starting materials and the presence of two new compounds, **1a** and **1b**, in an approximate 1:1 ratio. The solvent was next removed by vacuum, and purification was achieved by preparative TLC using a solvent mixture of CH_2Cl_2 and diethyl ether (30:1). Analytical samples of both new compounds were obtained by recrystallization from a 3:1 mixture of CH_2Cl_2 and hexane. Yields: **1a**, 0.017 g (25%); **1b**, 0.020 g (30%). The lowered yields are caused by partial decomposition of the products on the TLC plates. ^{1}H NMR ($CDCl_3$): for **1a**: δ 1.32 (s, 18H, *t*-Bu), 1.59 (s, 18H, *t*-Bu), 3.36 (s, 6H, OCH_3), 4.29 (d, J_{HH} = 12 Hz, 2H, CH_aH), 5.29 (d, J_{HH} = 12 Hz, 2H, $CH{H_b}$), 7.18 (d,

(37) Uchiyama, T.; Toshiyasu, Y.; Nakamura, Y.; Miwa, T.; Kawaguchi, S. *Bull. Chem. Soc. Jpn.* **1981**, *54*, 181−185.
(38) Doyle, J. R.; Slade, P. E.; Jonassen, H. B. *Inorg. Synth.* **1960**, *6*, 218.
(39) Myhre, P. C.; Beug, M.; James, L. L. *J. Am. Chem. Soc.* **1968**, *90*, 2105−2115.

J_{HH} = 4 Hz, 2H, C_6H), 7.51 (d, J_{HH} = 4 Hz, 2H, C_6H), 7.96 (s, 2H, NCH). ^{1}H NMR ($CDCl_3$): for **1b**: δ 1.31 (s, 18H, *t*-Bu), 1.55 (s, 18H, *t*-Bu), 3.33 (s, 6H, OCH_3), 4.33 (d, J_{HH} = 12 Hz, 2H, CH_aH), 5.13 (d, J_{HH} = 12 Hz, 2H, CHH_b), 7.18 (d, J_{HH} = 4 Hz, 2H, C_6H), 7.47 (d, J_{HH} = 4 Hz, 2H, C_6H), 8.02 (s, 2H, NCH). Anal. Calcd for **1a** ($C_{34}H_{52}O_2N_2PdCl_2$): C, 58.57; H, 7.52; N, 4.02. Found: C, 58.68; H, 7.58; N, 3.94. Calcd for **1b** ($C_{34}H_{52}O_2N_2PdCl_2$): C, 58.57; H, 7.52; N, 4.02. Found: C, 58.85; H, 7.59; N, 3.95.

Synthesis of $LPtCl_2$ (2a and 2b). To a 50 mL Schlenk flask containing 10 mL of chloroform (or toluene) were added 0.05 g (0.096 mmol) of glyoxal bis(2-(methoxymethyl)-4,6-di-*tert*-butylphenyl)imine (L) and 0.046 g (0.096 mmol) of $PtCl_2(PhCN)_2$, after which the reaction solution was heated to reflux for 2 h. The color of the reaction mixture changed from yellow to dark orange after 15 min. TLC analysis showed the disappearance of the starting materials and the presence of two major red spots corresponding to **2a** and **2b** in an approximate 1:1 ratio. The amount of the reaction solvent was reduced to by half via vacuum, and the products were precipitated from solution by the addition of hexane (20 mL). **2a** and **2b** were further separated by preparative TLC using CH_2Cl_2 as eluant. Analytically pure samples of both new compounds were obtained by recrystallization from a 1:3 mixture of CH_2Cl_2 and hexane. Yields: **2a**, 0.015 g (20%); **2b**, 0.017 g (23%). Like **1a** and **1b**, both **2a** and **2b** slowly decomposed on the TLC plates, which resulted in low yields. ^{1}H NMR ($CDCl_3$) for **2a**: δ 1.36 (s, 18H, *t*-Bu), 1.54 (s, 18H, *t*-Bu), 3.31 (s, 6H, OCH_3), 4.33 (d, J_{HH} = 12 Hz, 2H, CH_aH), 5.16 (d, J_{HH} = 12 Hz, 2H, CHH_b), 7.57 (d, J_{HH} = 4 Hz, 2H, C_6H), 7.78 (d, J_{HH} = 4 Hz, 2H, C_6H), 8.73 (s, 2H, NCH). ^{1}H NMR ($CDCl_3$) for **2b**: δ 1.35 (s, 18H, *t*-Bu), 1.53 (s, 18H, *t*-Bu), 3.31 (s, 6H, OCH_3), 4.40 (d, J_{HH} = 12 Hz, 2H, CH_aH), 5.10 (d, J_{HH} = 12 Hz, 2H, CHH_b), 7.27 (d, J_{HH} = 4 Hz, 2H, C_6H), 7.55 (d, J_{HH} = 4 Hz, 2H, C_6H), 8.74 (s, 2H, NCH). Anal. Calcd for **2a** ($C_{34}H_{52}O_2N_2PtCl_2{\cdot}CH_2Cl_2$): C, 48.23; H, 6.24; N, 3.21. Found: C, 48.72; H, 5.80; N, 3.69. Calcd for **2b** ($C_{34}H_{52}O_2N_2PtCl_2{\cdot}CH_2Cl_2$): C, 48.23; H, 6.24; N, 3.21. Found: C, 48.42; H, 5.90; N, 3.50.

Synthesis of $PdCl_2(LH_4)$ (3). To a colorless solution of 0.05 g (0.095 mmol) of LH_4 in 10 mL of CH_2Cl_2 was added 0.037 g (0.096 mmol) of $PdCl_2(PhCN)_2$, after which the reaction solution was stirred under room temperature for 2 h. TLC analysis showed the disappearance of the starting materials and the presence of desired compound **3** in almost quantitative yield. The solvent was removed by vacuum, and purification was achieved by passing the crude product through a short silica gel column using a mixture of CH_2Cl_2 and acetone (9:1). Yield: 0.065 g (96%). ^{1}H NMR ($CDCl_3$): δ 1.30 (s, 18H, *t*-Bu), 1.61 (s, 18H, *t*-Bu), 2.74 (m, 2H, NCH_a), 3.66 (s, 6H, OCH_3), 3.26 (m, 2H, NCH_b), 4.68 (d, J_{HH} = 12 Hz, 2H, CH_aH), 6.09 (s, 2H, NH), 7.29 (s, 2H, C_6H), 7.38 (s, 2H, C_6H), 7.62 (d, J_{HH} = 12 Hz, 2H, CH_aH). IR (KBr): 3363 (sh), 3320 (m) cm^{-1}. Anal. Calcd for $C_{34}H_{56}O_2N_2PdCl_2$: C, 58.24; H, 8.05; N, 3.99. Found: C, 58.38; H, 8.15; N, 3.88.

Synthesis of $PtCl_2(LH_4)$ (4). To a colorless solution of 0.05 g (0.095 mmol) of LH_4 in 10 mL of chloroform was added 0.046 g (0.096 mmol) of $PtCl_2(PhCN)_2$, after which the reaction solution was heated up to reflux for 2 h. Unlike **3**, **4** is not stable on TLC plates, so purification was performed by recrystallization of the crude material from a mixture of hexane and acetone (9:1) after removing the solvent by vacuum. Yield: 0.047 g (61%). ^{1}H NMR ($CDCl_3$): δ 1.27 (s, 18H, *t*-Bu), 1.62 (s, 18H, *t*-Bu), 2.74 (m, 2H, NCH_a), 3.61 (s, 6H, OCH_3), 3.74 (m, 2H, NCH_b), 4.64 (d, J_{HH} = 12 Hz, 2H, CH_aH), 7.28 (d, J_{HH} = 2 Hz, 2H, NH), 7.39 (d, J_{HH} = 2 Hz, 2H, C_6H), 7.66 (d, J_{HH} = 12 Hz, 2H, CHH_b). IR (KBr): 3353 (sh), 3317 (m) cm^{-1}. Anal. Calcd for $C_{34}H_{56}O_2N_2PtCl_2$: C, 51.63; H, 7.14; N, 3.54. Found: C, 51.67; H, 7.36; N, 3.25.

X-ray Crystallography. Crystals of **L**, **LH_4**, **2b**, **3**, and **4** were each mounted under Paratone-8277 on glass fibers and immediately placed on the X-ray diffractometer in a cold nitrogen stream supplied by a Siemens LT-2A low temperature device. The X-ray intensity data were collected on a standard Siemens SMART CCD area detector system equipped with a normal-focus molybdenum-target X-ray tube operated at 2.0 kW (50 kV, 40 mA). A total of 1321 frames of data (1.3 hemispheres) were collected using a narrow-frame method with scan widths of 0.3° in ω and exposure times of 10 s/frame for **L** and 30 s/frame for **LH_4**, **2b**, **3**, and **4** using a crystal-to-detector distance of 5.094 cm (maximum 2θ angle of 56.52°). The total data collection time was approximately 5 h for **L** and 12 h for **LH_4**, **2b**, **3**, and **4**. Frames were integrated with the Siemens SAINT program to yield the following: for **L**, a total of 4552 reflections, of which 1953 were independent (R_{int} = 2.19%, R_{sig} = 4.42%)[40] and 1559 were above 2$\sigma(I)$; for **LH_4**, a total of 6506 reflections, of which 2976 were independent (R_{int} = 3.85%, R_{sig} = 4.54%) and 2697 were above 2$\sigma(I)$; for **2b**, a total of 14525 reflections, of which 4958 were independent (R_{int} = 3.42%, R_{sig} = 4.26%) and 4237 were above 2$\sigma(I)$; for **3**, a total of 7930 reflections, of which 2915 were independent (R_{int} = 4.85%, R_{sig} = 5.98%) and 2440 were above 2$\sigma(I)$; for **4**, a total of 12954 reflections, of which 5067 were independent (R_{int} = 1.69%, R_{sig} = 4.42%) and 4868 were above 2$\sigma(I)$. The unit cell parameters, provided in Table 2, were based upon the least-squares refinement of three-dimensional centroids of >1500 reflections for each crystal. The space group assignments were made on the basis of systematic absences and intensity statistics[41] by using the XPREP program (Siemens, SHELXTL 5.04). The structures were solved by using direct methods and refined by full-matrix least-squares procedures on F^2. Although the frames were integrated to a maximum 2θ angle of 56.50° for **L**, **LH_4**, and **2b**, there were no observed data >45° and therefore these data were omitted from the refinement. Frames for **3** and **4** were integrated to maximum 2θ angles of 46.50 and 56.50°, respectively, and no data were omitted from the refinements. All non-hydrogen atoms were refined anisotropically, except the atoms of the solvent molecule in **2b** and **4,** giving data-to-parameter ratios >10:1. The CH_2Cl_2 molecule in **2b** was disordered over two sites, and refinement of the SOFs (site occupation factors) revealed the solvent to be half-occupied. All hydrogens were included in idealized positions, except the hydrogens of the disordered CH_2Cl_2 molecule in **2b**, which were not included. Final residuals and refinement parameters are provided in Table 2.

Acknowledgment. We wish to thank the National Science Foundation (Grant CHE 94-04991) for support of this work and Alfa/Aesar Johnson Matthey Co. Inc. for a generous loan of platinum and palladium salts.

Supporting Information Available: Tables of data collection and refinement parameters, non-H atomic coordinates, anisotropic thermal parameters, calculated hydrogen positional and isotropic thermal parameters, and complete bond distances and angles for non-hydrogen atoms (32 pages). Ordering information is given on any current masthead page.

OM970452T

(40) $R_{int} = \Sigma|F_o^2 - F_o^2(\text{mean})|/\Sigma[F_o^2]$; $R_{sigma} = \Sigma[\sigma F_o^2]/\Sigma[F_o^2]$.

(41) Intensity statistics from CCD data sets are often unreliable, especially for weakly diffracting crystals.